Sensors & Diagnostics

PAPER

View Article Online
View Journal | View Issue

Cite this: *Sens. Diagn.*, 2024, **3**, 1505

A nitroreductase-sensitive near-IR fluorescent biosensor for detecting tumor hypoxia *in vivo*†

Safiya Nisar and Binglin Sui *

Tumor cells have high metabolic demands, leading to increased oxygen consumption and further exacerbating hypoxia, which has been regarded as a characteristic feature of solid tumors and plays a significant role in tumor growth, resistance to therapy, and overall treatment outcomes. Hypoxia-specific sensing probes are currently in urgent need to provide valuable information for tumor detection and monitoring. In this work, we developed a new near-IR fluorescence-emitting biosensor with a high fluorescence quantum yield for hypoxia detection in tumor tissues. In the presence of nitroreductase enzyme under tumor hypoxia, the nitro group of the biosensor molecule is converted into an amino group, and the resulting compound turns itself into a nonfluorescent dye through a self-immolating process, thus turning off the fluorescence emission of the biosensor. The fluorescence change of the biosensor in response to nitroreductase is sensitive and selective and is not influenced by the presence of other physiologically important species. In the *in vitro* and *in vivo* bioimaging experiments, the biosensor demonstrated high efficiency in detecting hypoxia and the capability of distinguishing solid tumors of different sizes, indicating its potential applications in tumor diagnosis and progression monitoring.

Received 10th May 2024,
Accepted 21st July 2024

DOI: 10.1039/d4sd00146j

rsc.li/sensors

Introduction

Cancer, a multifaceted and relentless adversary, continues to pose a formidable challenge to modern medicine and scientific inquiry. In the realm of cancer, the pursuit of precision and insight has never been more critical. The recognition of hypoxia, or the lack of oxygen, as a fundamental characteristic of solid tumors has opened new avenues for understanding and treating cancer.[1–4] In hypoxic cells and tissues, the oxygen level varies from 0.02 to 2% (below 2.5 mmHg pO_2) in contrast to the up to ~9% (40 mmHg pO_2) oxygen concentration in normal cells and tissues.[5–7] The association between hypoxia and cancer progression, metastasis, and resistance to treatment has kindled an intense interest in understanding the molecular underpinnings of this phenomenon.[8–13] As the importance of hypoxia in cancer biology becomes increasingly evident, the need for sensitive, specific, and real-time detecting techniques has become paramount.

Nitroreductase (NTR), an enzyme expressed in hypoxic regions of tissues, has been found as a biomarker of tumor hypoxia due to its unique role in the presence of low-oxygen conditions.[14] The bonding of NTR and hypoxia presents an opportunity to not only better understand the disease but also develop novel diagnostic strategies, treatment modalities, and therapeutic targets. In this context, NTR-based hypoxia detection emerges as a promising and innovative technique that holds the potential to revolutionize our approach to cancer management. Meanwhile, NTR has been well recognized for its enzymatic capabilities, catalyzing the reduction of nitroaromatic compounds, which makes it a prime candidate for targeted drug delivery systems and innovative diagnostic strategies for solid tumors. By harnessing the enzymatic activities of NTR, various NTR-involved optical imaging techniques have been developed to detect hypoxia in the tumor microenvironment for cancer diagnosis.[15–22]

The development of near-infrared (NIR) fluorescence microscopy has revolutionized the field of biomedical imaging. The advantages of NIR fluorescence in bioimaging, including noninvasiveness, whole-body imaging, low tissue autofluorescence, deep tissue penetration, high signal-to-noise ratio, reduced phototoxicity, and enhanced resolution, have greatly expanded our ability to study and understand complex biological systems and have led to significant advancements in both basic research and clinical practice.[23–26] In this context, NIR fluorescent imaging of

Department of Chemistry, University of North Dakota, Grand Forks, ND 58202, USA. E-mail: binglin.sui@und.edu

† Electronic supplementary information (ESI) available: Synthesis and characterization of Cy7-NO_2 and related intermediates, UV-vis absorption and fluorescence emission spectra, the pH and temperature stability of the biosensor, the photostability of the biosensor, HRMS analysis of released species, the toxicity of Cy7-NO_2, confocal fluorescence images of Cy7-NO_2 in cancer cells. See DOI: **https://doi.org/10.1039/d4sd00146j**

nitroreductase emerges as a beacon of hope, casting light on the intricate tapestry of the tumor microenvironment with exceptional clarity. By coupling NTR activities with NIR fluorescence technology, we gain the ability to peer deep within biological tissues, directly detecting and visualizing hypoxia in tumors.

Herein, we intend to develop an NTR-based biosensor (Cy7-NO_2) emitting fluorescence in the NIR wavelength range for sensing tumor hypoxia. The biosensor is composed of a nitrobenzene ring, serving as the NTR-sensing unit, and an NIR fluorescent dye cyanine 7 (Cy7). Owing to its desired photophysical properties, Cy7 has been widely used to develop NIR fluorescent probes for various biological analytes, including hypoxia.[27–29] Analogous to Cy7, the biosensor emits strong fluorescence in nature. Different from previously reported hypoxia detection probes, which commonly display fluorescence OFF–ON response toward hypoxia, Cy7-NO_2 provides an alternative fluorescence ON–OFF mechanism. Also, this new biosensor has a straightforward molecular design, containing only the fluorophore and an aromatic nitro group, free of hydrolysable functional groups that were generally integrated in those hypoxia probes. Such an advantageous design eliminates potential interferences from some common enzymes in biological environments, such as esterases, proteases, ureases, and urethanases. As shown in Scheme 1, the nitro group of the biosensor is converted into an amino group in the presence of NTR under hypoxic conditions. The resulting compound turns itself into a nonfluorescent dye (Cy7-SH) through a self-immolating process, thus turning off the fluorescence emission of the biosensor.

Results and discussion

Synthesis of the biosensor Cy7-NO_2

As shown in Scheme 2, the synthesis of Cy7-NO_2 began with a commercially available chemical, 4-nitrobenzyl bromide, which reacted with potassium thioacetate to produce compound **1**. The acetyl group of **1** was removed by HCl to generate a thiol group in compound **2**. The fluorescent dye Cy7-Cl was prepared following a literature procedure (Scheme S1†).[30] The biosensor Cy7-NO_2 was obtained through a substitution reaction between Cy7-Cl and compound **2**, owing to the high reactivity of the *meso*-Cl of Cy7-Cl toward thiol groups. The chemical structure of Cy7-NO_2 was characterized by ^{1}H NMR (Fig. S1†), ^{13}C NMR (Fig. S2†), and HR-MS (Fig. S3†).

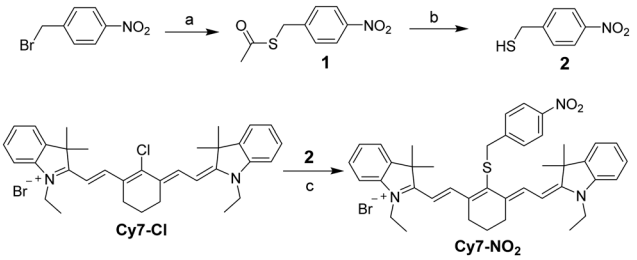

Scheme 2 Synthesis of the biosensor Cy7-NO_2. Reaction conditions: (a) KSAc, methanol, room temperature; (b) HCl, methanol, 60 °C; (c) DIEA, methanol, room temperature.

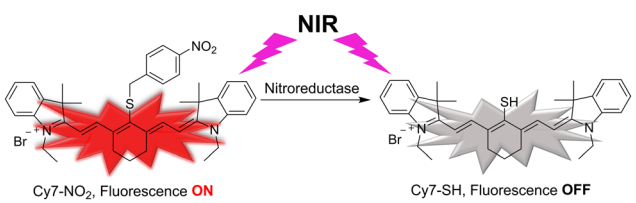

Scheme 1 Schematic illustration of the nitroreductase-induced fluorescence turn-off of the biosensor Cy7-NO_2. In the presence of nitroreductase, the arylnitro group of Cy7-NO_2 is reduced to an aniline group, which self-immolates to generate a non-fluorescent dye Cy7-SH, thus turning off the NIR fluorescence of the biosensor.

Photophysical properties of Cy7-NO_2

The photophysical properties of Cy7-NO_2 were measured by UV-vis spectroscopy and fluorescence spectroscopy. The biosensor showed a UV-vis absorption peak at 786 nm and a fluorescence emission maxima at 807 nm in the NIR wavelength region (Fig. S4†). Cy7-NO_2 emitted strong fluorescence with a fluorescence quantum yield determined to be 0.12 using indocyanine green as a reference.[31] Such an NIR fluorescence emission signal is adequate for *in vivo* bioimaging applications. Moreover, the fluorescence emission of Cy7-NO_2 was measured under conditions with different pH and varied temperatures. The recorded constant fluorescence intensity demonstrated its high stability over a wide range of pH values (Fig. S5†) and at physiological temperatures (Fig. S6†). In addition, the biosensor exhibited high photostability as evidenced by the nearly unchanged fluorescence emission intensity upon consecutive repeating excitations (Fig. S7†). These observations further confirmed its suitability for applications in biological environments.

Fluorescence response to nitroreductase

As a fluorescent biosensor for detecting hypoxic conditions of tumor microenvironments, Cy7-NO_2 was designed to display changes in its fluorescence properties in response to the existence of NTR. We studied the response function of the biosensor toward NTR by fluorescence spectroscopy. The fluorescence emission of Cy7-NO_2 was measured in DMSO-contained (10% by volume) phosphate-buffered solutions (PBS, pH 7.4) with and without NTR. β-Nicotinamide adenine dinucleotide (NADH) was used as an electron source to convert the aromatic nitro groups into amino groups. As shown in Fig. 1A, the fluorescence emission spectrum of Cy7-NO_2 (10 μM) exhibited nearly no change in PBS solutions after the addition of 1 mM NADH. However, upon adding 2.5 μg mL^{-1} NTR in the presence of 1 mM NADH, the fluorescence emission of Cy7-NO_2 was drastically quenched, and negligible fluorescence signals were detected after 20

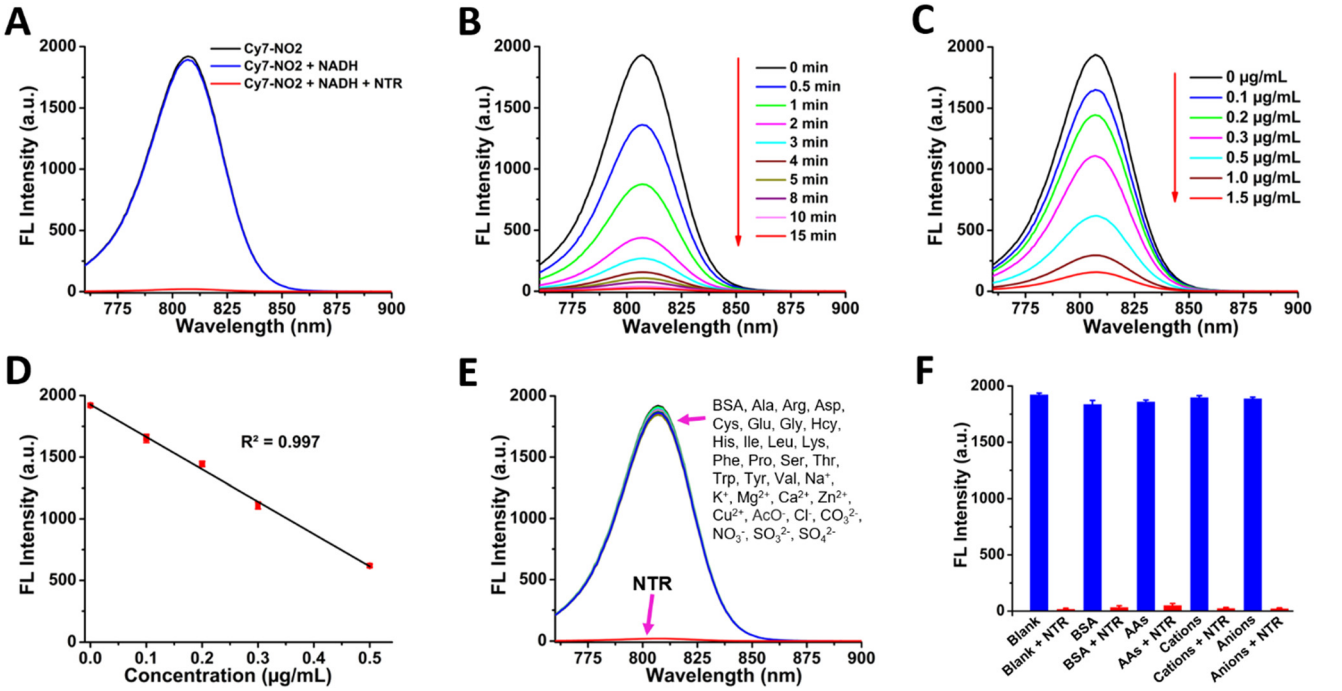

Fig. 1 (A) Fluorescence emission spectra of Cy7-NO_2 (10 μM) in the presence of NADH (1 mM), followed by the addition of NTR (2.5 μg mL^{-1}). (B) Time-dependent fluorescence emission of Cy7-NO_2 (10 μM) after the addition of NADH (1 mM) and NTR (2.5 μg mL^{-1}). (C) Fluorescence emission spectra of Cy7-NO_2 (10 μM) in the presence of NADH (1 mM) and NTR at varied concentrations; and (D) a plot of the fluorescence intensity and NTR concentration at low concentrations of NTR (≤0.5 μg mL^{-1}). (E) Fluorescence emission spectra of Cy7-NO_2 (10 μM) in the presence of NADH (1 mM) and various biologically related species, including NTR (2.5 μg mL^{-1}), BSA (10 μg mL^{-1}), and common amino acids at the concentration of 10 mM, and cations and anions at the concentration of 1 mM. (F) Fluorescence intensity of Cy7-NO_2 (blank: 10 μM Cy7-NO_2 + 1 mM NADH) upon adding NTR (2.5 μg mL^{-1}) in the absence and presence of BSA (10 μg mL^{-1}), mixed amino acids (AAs, 1 mM for each), mixed cations (0.5 mM for each), and mixed anions (0.5 mM for each).

min. The fluorescence quenching of the biosensor indicated the effectiveness of NTR in catalyzing the reduction of arylnitro groups. Besides, a time-dependent fashion was observed in the fluorescence turn-off process (Fig. 1B and S8†). These results consolidated the eligibility of Cy7-NO_2 in reflecting the existence of NTR under hypoxic conditions.

Nitroreductase detection sensitivity and the detection limit

To evaluate the sensitivity of Cy7-NO_2 in responding to NTR, we measured its fluorescence emission in PBS buffer solutions containing 1 mM NADH and NTR at different concentrations (0–1.5 μg mL^{-1}). Upon the addition of NTR, the fluorescence intensity of Cy7-NO_2 was decreased to varying degrees after 5 min, depending on the amount of added NTR (Fig. 1C). Furthermore, as shown in Fig. 1D, a linear relationship was observed between the fluorescence intensity of Cy7-NO_2 and the NTR concentration at low concentrations of NTR (≤0.5 μg mL^{-1}). The detection limit of the biosensor was determined to be 7.8 ng mL^{-1}.

Nitroreductase selectivity of Cy7-NO_2

In addition to NTR, the fluorescence responses of Cy7-NO_2 toward other biologically related species were also examined to reveal its selectivity in nitroreductase detection. As shown in Fig. 1E, the addition of bovine serum albumin (BSA, 10 μg mL^{-1}), common amino acids (Ala, Arg, Asp, Cys, Glu, Gly, Hcy, His, Ile, Leu, Lys, Phe, Pro, Ser, Thr, Trp, Tyr, and Val; 10 mM), cations (Na^+, K^+, Mg^{2+}, Ca^{2+}, Zn^{2+}, and Cu^{2+}; 1 mM), and anions (AcO^-, Cl^-, CO_3^{2-}, NO_3^-, SO_3^{2-}, and SO_4^{2-}; 1 mM) induced little to no changes in the fluorescence intensity of Cy7-NO_2 (with 1 mM NADH), which suggested the excellent selectivity of the biosensor.

Moreover, we studied the possible interference caused by the abovementioned species toward the NTR detection of Cy7-NO_2. The addition of NTR to Cy7-NO_2 solutions (with 1 mM NADH) containing BSA (10 μg mL^{-1}), mixed amino acids (a combination of Ala, Arg, Asp, Cys, Glu, Gly, Hcy, His, Ile, Leu, Lys, Phe, Pro, Ser, Thr, Trp, Tyr, and Val; 1 mM for each), mixed cations (a combination of Na^+, K^+, Mg^{2+}, Ca^{2+}, Zn^{2+}, and Cu^{2+}; 0.5 mM for each), or mixed anions (a combination of AcO^-, Cl^-, CO_3^{2-}, NO_3^-, SO_3^{2-}, and SO_4^{2-}; 0.5 mM for each) generated drastic fluorescence quench. As shown in Fig. 1F, the fluorescence changes in those solutions were comparable to that of the blank solution (10 μM Cy7-NO_2 + 1 mM NADH). These results evidenced that the NTR-specific fluorescence response of Cy7-NO_2 was not interfered by the existence of other biologically related species, suggesting the high reliability of the biosensor for NTR detection.

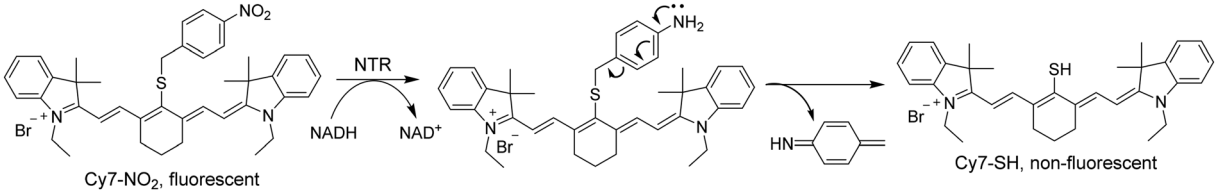

Fig. 2 Mechanism of the NTR-activated conversion of fluorescent Cy7-NO_2 to non-fluorescent Cy7-SH.

Mechanism of the nitroreductase-induced fluorescence turn-off

As explained in the introduction section, NTR is a highly efficient enzyme for catalyzing the reduction of arylnitro groups to convert them into aniline groups. Fig. 2 illustrates the mechanism of NTR activation of the biosensor Cy7-NO_2. Upon NTR-catalyzed reduction of the nitro group, with NADH as the electron supplier, the resulting 4-methylene aniline group self-eliminated into a stable molecule 4-methylenecyclohexa-2,5-dienimine, releasing a *meso*-thiol cyanine derivative Cy7-SH. As a result, the fluorescent Cy7-NO_2 was converted to the nonfluorescent Cy7-SH, leading to the turn-off of the fluorescence. HR-MS analysis of the final solutions of Cy7-NO_2 in the NTR detection experiments verified the formation of Cy7-SH (Fig. S9†), corroborating the plausibility of the mechanism.

Toxicity of Cy7-NO_2

Since the biosensor is expected to be utilized for detecting hypoxia in tumor tissues, the toxicity of Cy7-NO_2 was evaluated in human lung cancer A549 cells by the 3-(4,5-dimethylthiazol-2-yl)-2,5-diphenyl tetrazolium bromide (MTT) assay. After incubation in fresh cell culture media containing Cy7-NO_2 at varying concentrations (0–20 μM) for 24 h, the viability of cells was barely affected in comparison to cells treated with only fresh cell culture medium in the control group (Fig. S10†), which suggested the high biocompatibility of the biosensor. Therefore, Cy7-NO_2 has the potential to be exploited as a practical NIR fluorescent biosensor for hypoxia-detecting applications in physiological environments.

In vitro hypoxia detection in live cells

The biosensor was exploited for detecting hypoxia by means of intracellular NTR activities in A549 cells, which overexpress the NTR enzyme under hypoxic conditions,[18,19] using confocal laser scanning microscopy (CLSM). After incubation with 5 μM Cy7-NO_2 for 3 h, cells emitted striking fluorescence, indicating the cellular uptake of Cy7-NO_2 by cells (Fig. S11†). To study the hypoxia-detecting ability of the biosensor, cells were incubated with Cy7-NO_2 under hypoxic conditions (1% O_2) and normoxic conditions (20% O_2). For hypoxia detection, cells were cultured under low oxygen conditions for 6 h, which allowed them to generate a sufficient amount of NTR, mimicking the hypoxic microenvironment in tumor tissues. Then cells were incubated with Cy7-NO_2 for 15 min while maintaining the low oxygen condition. As shown in Fig. 3A, cells treated under normoxic conditions emitted strong fluorescence, whereas inconsiderable fluorescence emission was detected in cells under hypoxia, demonstrating that the fluorescence of Cy7-NO_2 was efficiently turned off by the NTR generated in cells under hypoxic conditions.

To further verify that the fluorescence decrease resulted from hypoxia-induced nitroreductase enzyme, cells were pretreated with 0.1 mM dicoumarin, which has been proven an effective inhibitor of the enzyme,[32,33] for 30 min prior to the incubation with Cy7-NO_2 for 15 min under hypoxic conditions. As shown in Fig. 3B, dicoumarin-pretreated cells under hypoxic conditions emitted strong fluorescence comparable to those under normoxic conditions. The unaffected fluorescence emission of Cy7-NO_2 was ascribed to the inhibition of the enzymatic activities of NTR by dicoumarin. These findings elucidated the NTR-based hypoxia-detecting capability of the biosensor.

In vivo tumor hypoxia detection in mice

Encouraged by the desirable behaviors of Cy7-NO_2 in detecting hypoxia *in vitro*, we further applied the biosensor to hypoxia detection in solid tumors of mice. A xenograft tumor model of A549 cancer was established in nude mice. Upon intratumoral injection of Cy7-NO_2 (10 μM, 20 μL), mice were imaged under anesthesia by a noninvasive *in vivo* Lago X imaging system (λ_{ex} = 790 nm, λ_{em} = 830 nm). As shown in Fig. 4A, intense fluorescence signals were recorded immediately. Afterward, the fluorescence intensity decreased rapidly, and negligible fluorescence emission was observed in

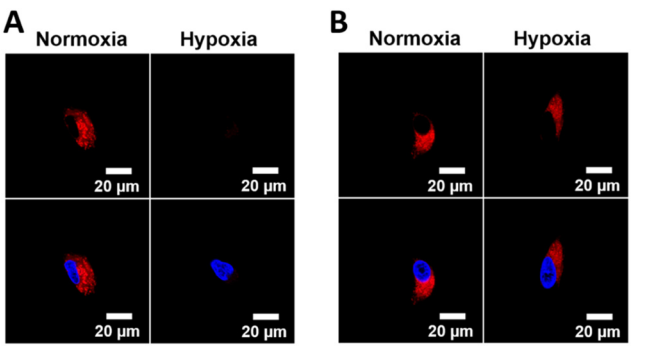

Fig. 3 CLSM images of (A) A549 cells and (B) dicoumarin-pretreated A549 cells under hypoxic and normoxic conditions. Cell nuclei were stained with DAPI. The blue and red fluorescence is from DAPI and Cy7, respectively.

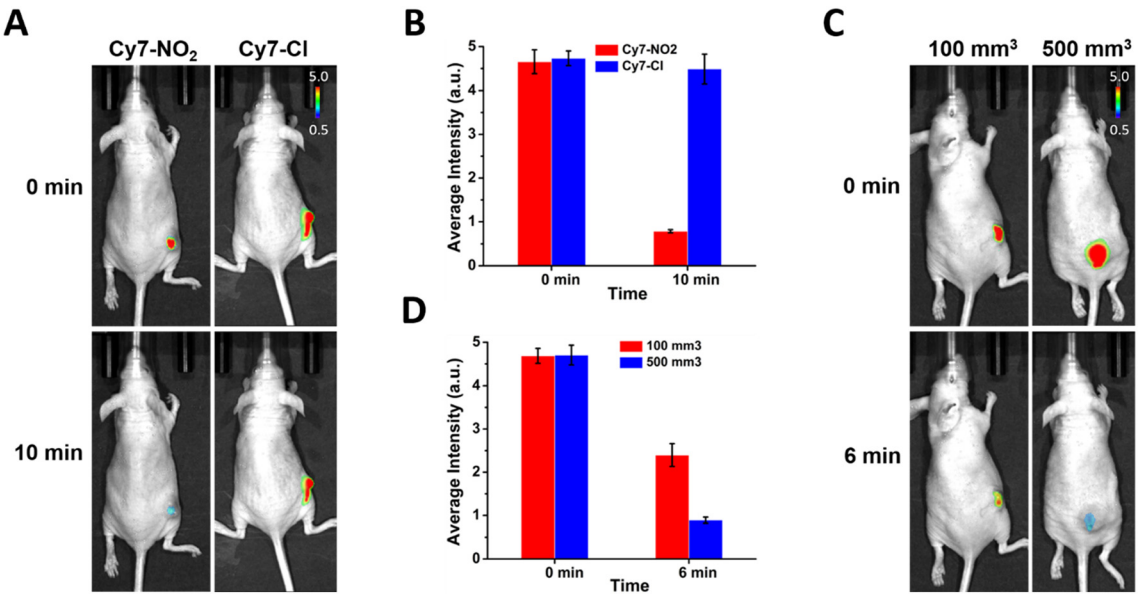

Fig. 4 *In vivo* tumor hypoxia imaging in mice bearing human lung A549 xenograft tumor. (A) Whole-body fluorescence images and (B) the corresponding average fluorescence intensity of mice upon intratumoral injection of Cy7-NO_2 and Cy7-Cl immediately (0 min) and after 10 min. (C) Fluorescence images and (D) the corresponding average fluorescence intensity of mice bearing tumors of different sizes (~100 mm^3 and ~500 mm^3) upon intratumoral injection of Cy7-NO_2 at 0 min and 6 min postinjection.

the tumor tissues within 10 min. To prove that the fluorescence turn-off of the biosensor resulted from tumor hypoxia, a hypoxia-irresponsive NIR fluorescent dye Cy7-Cl, which is the synthetic precursor of Cy7-NO_2 (Scheme 2), was used as a reference. Apparently, the tumor tissues injected with Cy7-Cl still emitted strong fluorescence after 10 min postinjection (Fig. 4A). The quantitative analysis of the fluorescence intensity further confirmed the efficiency of Cy7-NO_2 in responding to tumor hypoxia (Fig. 4B). Furthermore, we found that the fluorescence response of Cy7-NO_2 toward tumor hypoxia was related to the size of tumor solids. As shown in Fig. 4C, the fluorescence intensity of the biosensor decreased much faster in larger tumors (~500 mm^3) than in smaller ones (~100 mm^3) under the same conditions, which is in good agreement with the corresponding quantitative fluorescence intensity data (Fig. 4D). These observations demonstrated the ability of Cy7-NO_2 to distinguish solid tumors of varied sizes, which renders the biosensor potential to be exploited to estimate the malignancy of tumor lesions. All the experiment results indicated the suitability of Cy7-NO_2 as an efficient tool for hypoxic tumor detection *in vivo*.

Conclusion

An NIR fluorescence-emitting biosensor has been developed to efficiently detect tumor hypoxia *in vivo*. The new biosensor molecule consists of a cyanine fluorophore and a nitroreductase-sensitive arylnitro group. The biosensor exhibits selective fluorescence changes as a response to the nitroreductase enzyme but not to other physiologically related species, indicating its high selectivity in sensing nitroreductase. In the presence of the enzyme, the arylnitro group is reduced into an aniline group, which spontaneously self-immolates into a stable small molecule to release the fluorophore moiety as a nonfluorescent compound, thus turning off the fluorescence emission. Moreover, the optical response of the biosensor is not affected by the coexistence of other biological species. By means of the sensitive response to nitroreductase, the biosensor was successfully exploited to detect hypoxic conditions in cancer cells and solid tumors with high efficiency and distinguish tumors of different sizes, providing a valuable approach for studying hypoxia-related physiological activities in tumor tissues.

Materials and methods

Materials

Bromoethane, 2,3,3-trimethylindolenine, cyclohexanone, phosphorus oxychloride, sodium hydroxide, 4-nitrobenzyl bromide, potassium thioacetate, hydrogen chloride, *N*,*N*-diisopropylethylamine, phosphate-buffered saline (PBS), DL-dithiothreitol, paraformaldehyde, (3-(4,5-dimethylthiazol-2-yl)-2,5-diphenyltetrazolium) bromide (MTT), bovine serum albumin (BSA), and silica gel (spherical, 100 μm) were purchased from Thermo Fisher Scientific, Inc. (Waltham, MA, USA). Nitroreductase (NTR) and β-nicotinamide adenine dinucleotide (NADH) were purchased from EMD Millipore Corp. (Billerica, MA, USA). Gibco Dulbecco's modified Eagle's medium (DMEM), fetal bovine serum (FBS), penicillin–streptomycin (PS), trypsin-EDTA, and 4′,6-diamidino-2-phenylindole dihydrochloride (DAPI) were purchased from Thermo Fisher Scientific, Inc. (Waltham, MA, USA). Deuterated chloroform was purchased from Cambridge

Isotope Laboratories, Inc. (Andover, MA, USA). All of the solvents used in this research were purchased from Thermo Fisher Scientific, Inc. (Waltham, MA, USA) and directly used without further purification.

Photophysical properties

Spectroscopic properties of the biosensor were measured in 10 mm path length quartz cuvettes at room temperature. UV-vis absorption was measured with a PerkinElmer Lambda 1050 UV/vis/NIR spectrophotometer. Fluorescence emission spectra were obtained by using a Shimadzu RF-6000 spectrophotometer. All the measurements were conducted with an optical density no higher than 0.12 at excitation wavelength to avoid reabsorption. Fluorescence quantum yields were calculated by a standard relative method using the equation below with indocyanine green (ICG, $\Phi_{FL} \approx 0.13$ in ethanol) as a reference.

$$\Phi_{FL} = \Phi_R \frac{I}{I_R}\frac{OD_R}{OD}\frac{n^2}{n_R{}^2}\frac{RP_R}{RP}$$

where Φ is the quantum yield, the subscript R refers to the reference, I is the integrated emission signal, OD is the optical density at the excitation wavelength, n is the refractive index of the solvent, and RP is the relative power of the light source of the spectrofluorometer at the excitation wavelength.

Nitroreductase detection experiments

Stock solutions of NADH, NTR, BSA, amino acids (Ala, Arg, Asp, Cys, Glu, Gly, Hcy, His, Ile, Leu, Lys, Phe, Pro, Ser, Thr, Trp, Tyr, and Val), cations (Na^+, K^+, Mg^{2+}, Ca^{2+}, Zn^{2+}, and Cu^{2+}), and anions (AcO^-, Cl^-, $CO_3{}^{2-}$, $NO_3{}^-$, $SO_3{}^{2-}$, and $SO_4{}^{2-}$) were prepared in DI water at the concentration of 0.1 M. Stock solutions of Cy7-NO_2 with the concentration of 10 mM were prepared in DMSO and diluted with PBS buffer (pH 7.4). The UV-vis absorption and fluorescence emission spectra were measured in PBS solution (pH 7.4) with 10% DMSO (v/v). All samples were incubated in the dark at 37 °C for 3 h prior to measurements.

In the nitroreductase detection and titration experiments, the samples with predetermined concentrations of ingredients were prepared by mixing stock solutions of Cy7-NO_2 and other analytes. The resulting samples were incubated in the dark at 37 °C for 3 h and then measured by fluorospecroscopy (Shimadzu RF-6000 spectrophotometer).

Limit of detection measurement

The limit of detection (LOD) of the biosensor in detecting nitroreductase was determined according to the standard LOD calculation equation: $LOD = K \times \sigma/S$, where coefficient $K = 3$, σ is the standard derivation of the blank solution, and S is the slope of the calibration curve. The measurement at each concentration was repeated three times, and the average was used to plot the calibration curve.

Cell culture

Human lung cancer A549 cells were cultured in Dulbecco's modified Eagle's medium (DMEM, Gibco) supplemented with 10% FBS, 100 units mL^{-1} penicillin, and 100 μg mL^{-1} streptomycin at 37 °C in 100 mm cell culture dishes under a humidified atmosphere of 5% CO_2. Cells were subcultured when the cell confluence reached 70–80%.

Cell viability assay

The toxicity of Cy7-NO_2 was evaluated by the 3-(4,5-dimethylthiazole-2-yl)-2,5-diphenyltetrazolium ammonium bromide (MTT) assay. Cells were seeded at a density of 5000 cells per well in 96-well plates at 37 °C with 5% CO_2 for 24 h before the test. In the tests, cells were incubated with a fresh medium containing the biosensor at varied concentrations for 20 h. In the control group, cells were cultured in a fresh medium without any treatment. Thereafter, the medium was replaced with a solution of the MTT reagent in fresh medium at a concentration of 1 mg mL^{-1}, and the cells were incubated for another 4 h. The culture medium was carefully removed, and 100 μL of DMSO was added to each well of the plate. The plate was gently shaken to dissolve the purple crystals generated by the MTT reagent. The optical density at 570 nm was recorded on a microplate reader (BioTek Synergy H1 multimode microplate reader).

Confocal fluorescence imaging

Fluorescence images of cells were recorded by confocal laser scanning microscopy (CLSM). Cells were seeded at a density of 200 000 cells per dish in a 35 mm^2 Petri dish with a glass window at the bottom for 24 h at 37 °C with 5% CO_2 (+20% O_2 + 75% N_2). For confocal fluorescence imaging under hypoxic conditions, cells were incubated in an atmosphere with 5% CO_2 + 1% O_2 + 94% N_2. After being washed with PBS (pH 7.4), cells were incubated with the biosensor (5 μM). Cells cultured in a fresh medium without any incubation were used as a control. All cells were washed with PBS three times and fixed with paraformaldehyde (4% in PBS) for 10 min at room temperature. Following the removal of paraformaldehyde, cells were further washed with PBS thrice, and the nuclei of cells were stained with DAPI (final concentration 1 μg mL^{-1}) for 10 min. After three more times of washing with PBS, cells were imaged under a confocal microscope (Olympus FV3000 Laser Scanning Confocal Microscope).

Animal model

All animal experiments were conducted following NIH regulations and approved by the Institutional Animal Care and Use Committee of the University of North Dakota. A xenograft tumor model of A549 cancer was established in athymic BALB/c nude mice (8–10 weeks old, ~20 g, Jackson Laboratories). In brief, A549 cells suspended in DMEM culture medium (2 000 000 cells/100 μL) were inoculated

subcutaneously to mice. The tumor volume was measured by a digital caliper and calculated using the following formula: tumor volume = 0.5 × (tumor length) × (tumor width).[2] Tumor volumes were monitored every other day, and the animals were observed for body weight change and signs of pain throughout the experiments.

In vivo tumor hypoxia imaging

When the volume of tumors in tumor-bearing nude mice reached 100 mm^3, mice were randomly assigned into 3 groups (n = 5 for each group). All mice were marked and weighed prior to treatment. Mice were anesthetized with 2.5% isoflurane and then intratumorally administrated with sterilized saline (the control), Cy7-Cl, or Cy7-NO_2 solutions in saline. At predetermined post-administration time points, the whole body of mice was imaged under anesthesia by a noninvasive Lago X *in vivo* imaging system (Spectral Instruments Imaging Inc.). All images were collected under identical system settings.

Data availability

The data supporting this article have been included as part of the ESI.†

Conflicts of interest

The authors declare no competing financial interest.

Acknowledgements

We acknowledge the support from the National Science Foundation (CHE-2213445 and 2117699) and the University of North Dakota (the Early Career Scholars Award and the Postdoctoral Seed Funding). We also acknowledge the UND Behavioral Research Core Facility for animal studies.

References

1 A. L. Harris, Hypoxia — a Key Regulatory Factor in Tumour Growth, *Nat. Rev. Cancer*, 2002, **2**(1), 38–47.
2 A. Emami Nejad, S. Najafgholian, A. Rostami, A. Sistani, S. Shojaeifar, M. Esparvarinha, R. Nedaeinia, S. Haghjooy Javanmard, M. Taherian, M. Ahmadlou, R. Salehi, B. Sadeghi and M. Manian, The Role of Hypoxia in the Tumor Microenvironment and Development of Cancer Stem Cell: A Novel Approach to Developing Treatment, *Cancer Cell Int.*, 2021, **21**(1), 62.
3 Z. Chen, F. Han, Y. Du, H. Shi and W. Zhou, Hypoxic Microenvironment in Cancer: Molecular Mechanisms and Therapeutic Interventions, *Signal Transduction Targeted Ther.*, 2023, **8**(1), 70.
4 X. Jing, F. Yang, C. Shao, K. Wei, M. Xie, H. Shen and Y. Shu, Role of Hypoxia in Cancer Therapy by Regulating the Tumor Microenvironment, *Mol. Cancer*, 2019, **18**(1), 157.
5 J. M. Brown and W. R. Wilson, Exploiting Tumour Hypoxia in Cancer Treatment, *Nat. Rev. Cancer*, 2004, **4**(6), 437–447.
6 J. A. Bertout, S. A. Patel and M. C. Simon, The Impact of O_2 Availability on Human Cancer, *Nat. Rev. Cancer*, 2008, **8**(12), 967–975.
7 W. R. Wilson and M. P. Hay, Targeting Hypoxia in Cancer Therapy, *Nat. Rev. Cancer*, 2011, **11**(6), 393–410.
8 Y. Ye, Q. Hu, H. Chen, K. Liang, Y. Yuan, Y. Xiang, H. Ruan, Z. Zhang, A. Song, H. Zhang, L. Liu, L. Diao, Y. Lou, B. Zhou, L. Wang, S. Zhou, J. Gao, E. Jonasch, S. H. Lin, Y. Xia, C. Lin, L. Yang, G. B. Mills, H. Liang and L. Han, Characterization of Hypoxia-Associated Molecular Features to Aid Hypoxia-Targeted Therapy, *Nat. Metab.*, 2019, **1**(4), 431–444.
9 I. Dagogo-Jack and A. T. Shaw, Tumour Heterogeneity and Resistance to Cancer Therapies, *Nat. Rev. Clin. Oncol.*, 2018, **15**(2), 81–94.
10 C.-C. Huang, W.-T. Chia, M.-F. Chung, K.-J. Lin, C.-W. Hsiao, C. Jin, W.-H. Lim, C.-C. Chen and H.-W. Sung, An Implantable Depot That Can Generate Oxygen in Situ for Overcoming Hypoxia-Induced Resistance to Anticancer Drugs in Chemotherapy, *J. Am. Chem. Soc.*, 2016, **138**(16), 5222–5225.
11 W. H. Chang and A. G. Lai, The Hypoxic Tumour Microenvironment: A Safe Haven for Immunosuppressive Cells and a Therapeutic Barrier to Overcome, *Cancer Lett.*, 2020, **487**, 34–44.
12 B. Wang, Q. Zhao, Y. Zhang, Z. Liu, Z. Zheng, S. Liu, L. Meng, Y. Xin and X. Jiang, Targeting Hypoxia in the Tumor Microenvironment: A Potential Strategy to Improve Cancer Immunotherapy, *J. Exp. Clin. Cancer Res.*, 2021, **40**(1), 24.
13 R. Bai, Y. Li, L. Jian, Y. Yang, L. Zhao and M. Wei, The Hypoxia-Driven Crosstalk between Tumor and Tumor-Associated Macrophages: Mechanisms and Clinical Treatment Strategies, *Mol. Cancer*, 2022, **21**(1), 177.
14 Y.-L. Qi, L. Guo, L.-L. Chen, H. Li, Y.-S. Yang, A.-Q. Jiang and H.-L. Zhu, Recent Progress in the Design Principles, Sensing Mechanisms, and Applications of Small-Molecule Probes for Nitroreductases, *Coord. Chem. Rev.*, 2020, **421**, 213460.
15 Y. Wang, X. Han, X. Zhang, L. Zhang and L. Chen, A High-Selectivity Fluorescent Probe for Hypoxia Imaging in Cells and a Tumor-Bearing Mouse Model, *Analyst*, 2020, **145**(4), 1389–1395.
16 A. Chevalier, Y. Zhang, O. M. Khdour, J. B. Kaye and S. M. Hecht, Mitochondrial Nitroreductase Activity Enables Selective Imaging and Therapeutic Targeting, *J. Am. Chem. Soc.*, 2016, **138**(37), 12009–12012.
17 K. H. Gebremedhin, Y. Li, Q. Yao, M. Xiao, F. Gao, J. Fan, J. Du, S. Long and X. Peng, Development of a Red-Light Emission Hypoxia-Sensitive Two-Photon Fluorescent Probe for in Vivo Nitroreductase Imaging, *J. Mater. Chem. B*, 2019, **7**(3), 408–414.
18 J. Xu, S. Sun, Q. Li, Y. Yue, Y. Li and S. Shao, A Rapid Response "Turn-On" Fluorescent Probe for Nitroreductase Detection and Its Application in Hypoxic Tumor Cell Imaging, *Analyst*, 2015, **140**(2), 574–581.
19 R. Wang, J. Chen, J. Gao, J.-A. Chen, G. Xu, T. Zhu, X. Gu, Z. Guo, W.-H. Zhu and C. Zhao, A Molecular Design Strategy

toward Enzyme-Activated Probes with Near-Infrared I and II Fluorescence for Targeted Cancer Imaging, *Chem. Sci.*, 2019, **10**(30), 7222–7227.

20 J. Zhang, H.-W. Liu, X.-X. Hu, J. Li, L.-H. Liang, X.-B. Zhang and W. Tan, Efficient Two-Photon Fluorescent Probe for Nitroreductase Detection and Hypoxia Imaging in Tumor Cells and Tissues, *Anal. Chem.*, 2015, **87**(23), 11832–11839.

21 S. Karan, M. Y. Cho, H. Lee, H. M. Kim, H. S. Park, E. H. Han, J. L. Sessler and K. S. Hong, Hypoxia-Directed and Self-Immolative Theranostic Agent: Imaging and Treatment of Cancer and Bacterial Infections, *J. Med. Chem.*, 2023, **66**(20), 14175–14187.

22 Y. Zhang, X.-F. Zhang, Q. Chen, X.-Q. Cao and S.-L. Shen, A Novel Near-Infrared Fluorescence Off-On Probe for Imaging Hypoxia and Nitroreductase in Cells and in Vivo, *Sens. Actuators, B*, 2022, **353**, 131145.

23 Z. Guo, S. Park, J. Yoon and I. Shin, Recent Progress in the Development of Near-Infrared Fluorescent Probes for Bioimaging Applications, *Chem. Soc. Rev.*, 2014, **43**(1), 16–29.

24 J. O. Escobedo, O. Rusin, S. Lim and R. M. Strongin, NIR Dyes for Bioimaging Applications, *Curr. Opin. Chem. Biol.*, 2010, **14**(1), 64–70.

25 C. Sun, W. Du, B. Wang, B. Dong and B. Wang, Research Progress of Near-Infrared Fluorescence Probes Based on Indole Heptamethine Cyanine Dyes in Vivo and in Vitro, *BMC Chem.*, 2020, **14**(1), 21.

26 J. Zhao, T. Ma, B. Chang and J. Fang, Recent Progress on NIR Fluorescent Probes for Enzymes, *Molecules*, 2022, **27**(18), 5922.

27 Y. Li, Y. Sun, J. Li, Q. Su, W. Yuan, Y. Dai, C. Han, Q. Wang, W. Feng and F. Li, Ultrasensitive Near-Infrared Fluorescence-Enhanced Probe for in Vivo Nitroreductase Imaging, *J. Am. Chem. Soc.*, 2015, **137**, 6407–6416.

28 J. Zheng, Y. Shen, Z. Xu, Z. Yuan, Y. He, C. Wei, M. Er, J. Yin and H. Chen, Near-infrared off-on fluorescence probe activated by NTR for in vivo hypoxia imaging, *Biosens. Bioelectron.*, 2018, **119**, 141–148.

29 Y. Li, Y. Deng, J. Liu, J. Fu, Y. Sun, R. Ouyang and Y. Miao, A near-infrared frequency upconversion probe for nitroreductase detection and hypoxia tumor in vivo imaging, *Sens. Actuators, B*, 2019, **286**, 337–345.

30 W. Wang, Z. Fang, X. Zhang, H. Cai, Y. Zhao, W. Gu, X. Yang and Y. Wu, A Self-Assembled "Albumin–Conjugate" Nanoprobe for Near Infrared Optical Imaging of Subcutaneous and Metastatic Tumors, *ACS Appl. Bio Mater.*, 2020, **3**(1), 327–334.

31 K. Rurack and M. Spieles, Fluorescence Quantum Yields of a Series of Red and Near-Infrared Dyes Emitting at 600–1000 nm, *Anal. Chem.*, 2011, **83**(4), 1232–1242.

32 R. L. Koder and A.-F. Miller, Steady-State Kinetic Mechanism, Stereospecificity, Substrate and Inhibitor Specificity of Enterobacter Cloacae Nitroreductase, *Biochim. Biophys. Acta*, 1998, **1387**(1), 395–405.

33 S. Chen, L. Xiao, Y. Li, M. Qiu, Y. Yuan, R. Zhou, C. Li, L. Zhang, Z.-X. Jiang, M. Liu and X. Zhou, In Vivo Nitroreductase Imaging via Fluorescence and Chemical Shift Dependent 19F NMR, *Angew. Chem., Int. Ed.*, 2022, **61**(50), e202213495.